Strojniški vestnik - Journal of Mechanical Engineering 70(2024)5-6, 231-246
DOI:10.5545/sv-jme.2023.776
Original Scientific Paper
Received for review: 2023-08-27
Received revised form: 2023-12-08
Accepted for publication: 2024-03-12
© 2024 The Authors. CC BY 4.0 Int. Licensee: SV-JME

The Influence of Pump-Turbine Specific Speed on Hydraulic Transient Processes

Zdravko Giljen[1,*] – Miloš Nedeljković[1] – Yongguang Cheng[2]
[1] University of Belgrade, Faculty of Mechanical Engineering, Serbia
[2] Wuhan University, State Key Laboratory of Water Resources and Hydropower Engineering Science, Wuhan, China

The main porpose of this paper is to perform and present at transient process analysis on the influence of different specific speeds (nq) of the three-model pump-turbines that may implemented at the hydropower pump storage plant (HPSP) Bajina Basta, Serbia. The intention is to analyze the operation regimes along the S-shaped characteristic curve, which creates difficulties in calculations during the load-rejection process. These problems are manifested by an unusual increase in water pressure, followed by an increase in machine vibrations, thus threatening the stability of machine operation. The subject of this research is the four-quadrant (4Q) characteristic curves, presented in the form of Suter curves (the head and momentum parameters (Wh and Wm), in dependence of angle (θ)) for different wicket gate openings, of the three pump-turbine models with different specific speeds (nq = 27, nq = 38 and nq = 50). These 4Q characteristics are used as input data for numerical code developed to calculate the simultaneous load rejection of both pump-turbines. The numerical code is based on the method of characteristics and applied to the test case at HPSP. This is especially relevant when dealing with characteristic S-shaped curves that may lead to serious instability in operation during the transient process. The calculation results show changes in the pressure, speed of rotation and discharge of the machine operation regimes, but the important findings are reflected in further application of the results to determine the parametric flow and speed (Q_{11} and n_{11}) trajectories of the operating points, where the unstable behavior of a pump-turbine operating in turbine mode is presented and periodically the trajectories also pass through the reverse pump zone.

Keywords: hydraulic transients, pump-turbine, influence of the specific speed, load rejection, working point trajectory, method of characteristics

Highlights

- *The authors developed a numerical code for calculating transient processes based on the method of characteristics (MOC) and used this code to compute the transient processes for the test case at HPSP Bajina Basta, Serbia, as well as to calculate the operating point trajectory during shutdown.*
- *This paper presents the analysis of results obtained during the calculated transient processes of the two pump-turbines (the changes in pressure in the spiral casing, the pressure in the draft tube, the speed of rotation, discharge, and wicket gate opening), and for the analysis of the impact of nq - specific speed on the transient processes.*
- *The 4Q characteristics in $Q_{11}/{}_oQ_{11o}$ – $n_{11}/{}_on_{11o}$ diagrams for both pump-turbines show the trajectory of working points during load rejection from a turbine zone. ${}_oQ_{11o}$ is the rated unit discharge [-], and ${}_on_{11o}$ is the rated unit speed of rotation [-].*
- *The analysis of the trajectory of the working point for all three pump-turbine models (nq = 27, nq = 38 and nq = 50) during the transient process, is especially analyzed.*

0 INTRODUCTION

The detailed study of the available literature in the field of hydraulic machines showed that a small number of research papers dealt with the problem of the influence of specific speed (*nq*) on the shape of four-quadrant (4Q) performance curves, and consequently on their application in the calculation of transient processes. This was the main motivation for writing this paper where the analysis of transition processes of load rejection in the hydropower plant Bajina Basta, Serbia was performed.

The operating characteristics of pump-turbines, which in certain zones have the form of the letter *S* can lead to a relatively large hydraulic shock and pulsating pressures. These pressures and the high velocity of runaway during transients can directly damage the pipelines and shorten the life of the turbine.

Four-quadrant (4Q) hydraulic machinery performance curves are required to calculate transients in hydraulic systems, and as a rule in the literature, such curves are given only for three specific speeds: *nq* = 25 *nq* = 147, and *nq* = 261 (one radial, one semi axial and one axial turbomachine, respectively, in SI system units). When needed for some other *nq*, the performance curves nearest to such *nq* are used, even without any interpolation. To date, the influences of different specific speeds corresponding to the performance curves of turbomachinery (pumps, pump-turbines, and turbines) on transient processes have been scarcely studied and analyzed. Certain contributions in this area have been reported **[1]** **to** **[5]**. This paper discusses this influence on the concrete

*Corr. Author's Address: University of Belgrade, Faculty of Mechanical Engineering, Kraljice Marije 16, 11120 Belgrade, Serbia, zgiljen@gmail.com

example of the pumped-storage plant (PSP) Bajina Basta (also known as a reversible hydropower plant, RHPP), where two pump-turbines are installed (2 × 315 MW; this is the maximum power output in turbine mode). The transition process analyzed herein refers to the simultaneous load rejection of pump-turbines working in turbine modes, the first one with a power of 281 MW, and the second one with a power of 284 MW.

For the calculation of transient processes, as the input data, the 4Q characteristics are represented by Suter curves (*Wh* and *Wm* diagrams, where *Wh* is the non-dimensional characteristic head, and *Wm* is the non-dimensional characteristic moment) for three pump-turbine models with specific speeds of $nq = 27$, $nq = 38$ and $nq = 50$. All three sets of Suter curves are shown in Figs. 3 to 8, for various openings of the wicket gates. The diagrams are obtained by calculating the 4Q characteristics from the non-dimensional curves experimentally determined for defined pump-turbine models (where Q_{11} is unit discharge [-], n_{11} unit speed of rotation [-], M_{11} unit moment [-]). The key steps in the process of converting the 4Q characteristics into the form of Suter curves are presented in more detail in **[6]**.

The authors developed a numerical code for calculating transient processes based on the method of characteristics (MOC) **[7]** and used this code to compute the transient processes for the test case at HPSP Bajina Basta, Serbia, as well as for the calculation of the operating point trajectory during shutdown.

The literature survey reveals that although a lot of authors investigated the behavior of hydraulics phenomena in the pump-turbines during the transient processes, a relatively small number of them studied the influence of specific speed on transient processes.

In Donsky **[1]**, the complete operating characteristics of pumps were used to determine the effects of transient processes, including a water hammer in the inlet and drainage lines, on the normal or abnormal starting and stopping of the pumps. The three 4Q characteristics available in the literature (by Knapp and Stepanoff) were compared, and the influence of the specific speed on the calculation of transient processes was presented. Regarding the power failure of the pumps, the transient processes determined that the 4Q characteristics have the most unfavorable impact when a pump with the lowest specific speed is used.

In Brown and Rogers **[2]**, pumps in the southern Nevada system were employed to reveal that the specific speed can influence the transient process calculations. Pumps from three different manufacturers with different 4Q characteristic curves were installed in this system. The pressure at the discharge side was measured for these three pumps; under identical power failure conditions, and there were differences in the measured results due to the influence of the specific speed on the transient processes.

Giljen and Nedeljkovic **[4]** analyzed a transient process for a defined pump installation, and the influence of the specific speed (*nq*) on the results obtained during the calculation was determined. In the numerical code for calculating the transient processes, the values for the *Wh* and *Wm* characteristic curves obtained from model tests and from the originally derived universal equations for *Wh* and *Wm* were used for seven radial pump-turbine models and one radial pump model. A separate MATLAB program was utilized to obtain the Suter curves from the performance characteristics of these models and to establish universal equations (universal curves).

In Li et al. **[8]** 3D numerical simulations were carried out by the commercial software STAR-CCM+ to investigate the hydraulic transient and flow behaviors of a prototype pump-turbine during the normal shutdown process. The global characteristics and pressure fluctuations were analyzed as the pump-turbine run through the turbine mode, into the turbine braking mode, and finally into the reversed pump mode. Giljen **[9]** presented the transient process calculation results for the prototype Francis turbine installed at the hydropower plant (HPP) Piva. Giljen **[10]** also investigated and compared the pressure fluctuations in the draft tube of the prototype Francis turbine installed at HPP Piva during full load rejection. Capponi et al. **[11]** calculated transient processes by two different numerical models: first, the MOC was employed, and second, a frequency-domain model was developed as an impedance method (IM) model. Casartelli et al. **[12]** presented the computations of three different dynamic pump-turbine operating conditions. The results, using steady boundary conditions (BC) in the unstable region as well as transient BC like load-rejection and runaway, were computed with EARSM, showing its superiority compared to linear two equation models. Deniz et al. **[13]** focused on the flow instabilities of pump-turbines. The results of the experiments and computational fluid dynamics (CFD) simulations of the research carried out on a low-specific speed model pump-turbine are presented. In Fu et al. **[14]** the load rejection transient process of a pump-turbine was simulated with a three-dimensional (3D) large eddy simulation method and a dynamic mesh technology.

The simulation results were validated against the experimental data. In Xia et al. [15] the load rejection processes of two model pump-turbines with the same specific-speed but different in the runner blade inlet shape were investigated by a 3D numerical simulation method, were analyzed. Zheng et al. [16] presented the influences of rotational speed variations on the vibration performances of the whole unit with reversible pump-turbine (including the top cover, the upper and the lower brackets). The phenomenon is experimentally investigated with discussions of their sources and propagation characteristics, during the spin-no-load mode. Xia et al. [17] performed the analysis of the evolution of flow structures and pressure fluctuations in the S-shaped region of pump-turbines, and 3D numerical simulations were carried out for a model pump-turbine at four different guide-vane openings (GVOs). Hu et al. [18] performed an analysis of the hydraulic characteristics of pump-turbines in off-design conditions, especially the S-shaped characteristics, which are crucial for the safety and stability of the unit. To explore the *S*-characteristics of pump-turbines through a transient method, an experimental investigation was conducted based on a pumped-storage model system. Li et al. [19] performed an analysis of transient processes of a flow rate that increased and decreased in the pump mode of a model pump-turbine that were simulated through unsteady simulations using the shear stress transport (SST) k–ω turbulence model. Pump performance characteristics of pump-turbines in transient processes are significantly different from those in steady processes and are analyzed in this paper. Zhang et al. [20] performed the analysis of the pressure pulsations in the vaneless space of pump-turbines, which are extremely intense and always experience rapid time variations during transient scenarios, causing structural vibrations and even more serious accidents. The mechanism behind the rapid time variations of the vaneless space pressure pulsations in a model pump-turbine during runaway was analyzed through 3D numerical simulations. Zhu et al. [21] analyzed the two pump-turbine runners, one with a large positive blade lean and the other with a large negative lean, which are investigated numerically and experimentally. Frequent changes in the operating modes pose significant challenges in the development of a pump-turbine with high efficiency and stability. Fu et al. [22] analyzed the complex energy conversion and energy dissipation that occur in pump-turbines during the load rejection process. 3D transient turbulent flow in a pump-turbine was simulated using the method of coupling the rigid rotor motion with flow and dynamic mesh technology. Ran and Luo [23] performed the experiments in a medium specific-speed pump-turbine scaled model to investigate instability characteristics in pump mode, namely the head-drop phenomena. Two different head-drops are captured on a pump performance curve. The experimental investigations of the head-drop phenomenon, with the flowrate varying from 0.6 to 0.7 times of the design flowrate in the scaled model has also been presented. In Xiuli et al. [24] the transient flow characteristics are analyzed for a Francis-type reversible pump-turbine in generating mode by 3D numerical simulation with a moving mesh technique using the detached eddy simulation (DES) turbulent model. Yexiang et al. [25] analyze the S-shaped characteristic curves of pump-turbines that complicate synchronization with the electrical grid and affect system safety. Misaligned guide vanes (MGVs) are one of the most effective solutions to avoid S-shaped characteristics. Xia et al. [26] analyzed the understanding of the formation mechanism of the S-shaped characteristics (SSCs) and the relationship between flow structures and the runaway instability (RI), to optimize runner design for the promotion of operational reliability and flexibility. A new turbine equation is derived to reveal the prime cause of the SSCs, and the influence of geometric parameters on the SSCs was analyzed. Xia et al. [27] analyzed the pressure fluctuations and runner loads during the runaway process on a model pump-turbine runner at four guide vane openings (GVOs) using 3D (-CFD). In Li et al. [28] similarities of the flow in the rotor–stator interaction (RSI) affected region (stay vanes, guide vanes, and runner domain) in the prototype and the model Francis pump-turbines were analyzed, using numerical simulations with special attention to the influence of the Reynolds number. Zhang et al. [29] performed the analysis of the transient process, when hydro turbines may demonstrate some dynamic characteristics that differ from the corresponding static characteristics in steady operating conditions. Zeng et al. [30] analyzed the way that during the transitional processes of load rejection in a pumped-storage station, the S-shaped characteristics of the pump-turbines can result in relatively large water-hammer and pulsating pressures. These pressures and the high runaway speed during transient processes may directly damage the penstocks and shorten the life of the turbine. In that paper, different guide-vane closing schemes for reducing the maximum transient pressures, including the water-hammer and pulsating pressures, and runaway speed were investigated, and the principles for improving the closing schemes were

theoretically analyzed based on the transient characteristics in the *S*-shaped region. Cavazzini et al. [31] present a numerical aS-nalysis of the unstable behavior of a pump-turbine operating in turbine mode near the no-load condition. To study the unsteady phenomena which lead to the S-shape of the turbine characteristic, a load rejection scenario at constant and large guide vane opening was numerically analyzed by running through the flow-speed characteristic up to the turbine brake region. Zeng et al. [32] analyzed the way that pump-turbine characteristics greatly affect the operational stability of pumped-storage plants. In particular, the S-shaped region of the characteristic curves leads to severe instability during runaway conditions with servomotor failure. They investigated the runaway stability criterion by considering all the important effects in the hydro-mechanical system. Yu et al. [33] performed an analysis based on a numerical simulation of hydraulic transients in a PSP, and different closure laws were investigated for use when a high-head pump-turbine load rejection occurs. Sun et al. [34] analyzed the way that pump-turbine operation along the S-shaped curve can lead to difficulties in the load rejection process with unusual increases in water pressure. Pressure fluctuations are the primary reason for unstable operation of pump-turbines. Misaligned guide vanes (MGVs) are widely used to control the stability in the S-shaped region. Huang et al. [35] made a significant contribution when, they developed a method for predicting the complete four-quadrant characteristics of the Francis pump-turbine. A mathematical model was developed that describes the complete four-quadrant characteristics of the Francis pump-turbine, and Euler's equations and speed triangles on the impellers were used as the basis for developing this mathematical model. The most important contribution of that paper is reflected in the combination of the developed mathematical model with the regression analysis of characteristic operating points (COPs), and based on these the complete four quadrant characteristic curves for arbitrary specific speed are predicted. Pejovic et al. [36] analyzed the transient processes on reversible pump-turbine units, which were caused by a sudden load shedding of one or two reversible pump-turbine units. The authors of this paper also performed an analysis of the operation of the pump-turbine in the area where resonance can occur due to the instability of the pump and turbine in the runaway zone. They concluded that in hydropower plants with pump turbines of high capacity and high head, serious pressure fluctuations and dynamic stresses occur in certain parts of the plant. They also concluded that any asymmetry in aggregates, such as different loads, differences between the pump-turbine and the engine-generator, differences in the closing process of the intake valve and wicket gates of the conducting apparatus, asymmetry in the layout of the hydroelectric power plant constructions, etc., causes a phase shift. and, due to instability, significantly increased amplitude of pressure pulsations. Zeng et al. [37] designed a set of the four-quadrant characteristics of pump-turbines, which is of great importance, when the corresponding four-quadrant characteristics of pump-turbines cannot be used for replacement at the same specific speed. A major contribution of this paper is reflected in the newly developed method for the characterization of the pump turbines at any specific speed using a database of 25 available sets of the four-quadrant characteristics of pump turbines. The authors of this paper verified the developed method by comparing it with the measured four-quadrant characteristic curves of pump turbines with reasonable accuracy. Meniconi et al. [38] performed certain tests in water distribution networks and performed an analysis of the relevance of system configuration, energy dissipation phenomena, and pipe material characteristics in a real transmission network during the transient process. The aim was to create a numerical model that was progressively refined not only in terms of the governing equations but also by including more and representing the layout of the system and considering the actual functioning of the conditions. As a result, the unexpected role of smaller branches of the pipeline systems, i.e., pipes less than 1 % of the length of the main pipe – was indicated and a preliminary criterion for the system skeletonization was offered. Moreover, the importance of unsteady friction and viscoelasticity was assessed as a prominent remarkable effect of small defects. Simpson and Marchi [39] performed a detailed analysis of affinity laws relating to the four-quadrant characteristics of pumps operating at different speeds, and in the context of water distribution, affinity laws are commonly used to predict the pump curve for variable speed pumps. The research reported in this paper estimates the efficiency error for a wide range of pump sizes and tests the use of the previously proposed formula as an alternative to the affinity laws. The results show that a better estimate of the efficiency of small and medium pumps can be achieved with this formula. Moreover, the main contribution is that the formula can be easily implemented in hydraulic solvers. Zhou et al. [40] performed a detailed analysis of cavitation on the centrifugal pumps. They observed that cavitation produces a deterioration of the

hydraulic performance of centrifugal pumps. They also performed an analysis to prevent or reduce the damage it causes the cavitation on the centrifugal pump with an inducer and splitter blades. Soori and Asmael [41] performed an analysis showing that machining force and machining temperature can cause deflection errors in the machined turbine blades, and this effect needs to be minimized to increase the accuracy of machined blades. Their paper presented the application of a virtual machining system to predict and minimize the residual stress and deflection error in five-axis milling operations of turbine blades.

This paper presents the analysis of results obtained during the calculated transient processes of the two pump-turbines (the changes in pressure in the spiral casing, pressure in the draft tube, speed of rotation, discharge, and wicket gate opening). The 4Q characteristics in $Q_{11}/_{o}Q_{11o}$and $n_{11}/_{o}n_{11o}$ diagrams for both pump-turbines show the trajectory of working points during load rejection from a turbine zone. $_{o}Q_{11o}$ is the rated unit discharge [-] and $_{o}n_{11o}$ is the rated unit speed of rotation [-] The analysis of the trajectory of the working point for all three pump-turbine models (nq = 27, nq = 38 and nq = 50) during the transient process, is especially closely analyzed. The transient process was started in the turbine mode; thereafter the working point is moving from the turbine zone (III) to the reverse pump zone (IV). During this period the pump-turbines operated along the characteristic where the curve has an S-shape, which leads to difficulties during the load-rejected process manifested by an unusual increase in water pressure (for pump-turbine 1 a maximum head in the spiral casing of 940 m, 1175 m, and 1025 m were calculated for nq = 27, nq = 38, and nq = 50, respectively, while for pump-turbine 2 a maximum head in the spiral casing of 943 m, 1085 m, and 1010 m were calculated for nq = 27, nq = 38 and nq = 50, respectively). This leads to an increase in machine vibrations and threatens the stability of the machine. In-depth analysis on how much specific speed nq has a negative impact on this behavior is the main contribution of the paper.

1 DESCRIPTION OF PSP BAJINA BASTA

The first unit at HPSP Bajina Basta, was commissioned in June 1980, at that time, this PSP had the largest head in the world at 600 m. The HPSP is an accumulation-derivation plant with its upper reservoir located in Tara Mountain and its lower reservoir in the Drina River, which is the accumulation source for PSP. The connection between the upper and lower reservoirs is through a pipeline system, and the powerhouse is equipped with two pump-turbines.

The pipeline system consists of the following components: an upper entrance-exit building, located in the upper reservoir; an 8-km-long tunnel (6.3 m in diameter) that connects the upper reservoir to the upper penstock; a surge tank with a height of 141 m; a penstock valve; an underground upper penstock (consisting of a sloped part 738 m long and 4.8 m in diameter inclined at an angle of 45° and a horizontal part 635 m long and 4.2 m in diameter) that connects the pipeline to the pump-turbines and machine power house; a lower penstock (314 m long and 7 m in diameter) partly housed underground and partly passing through the existing dam that connects the machine power house to the lower exit-entrance

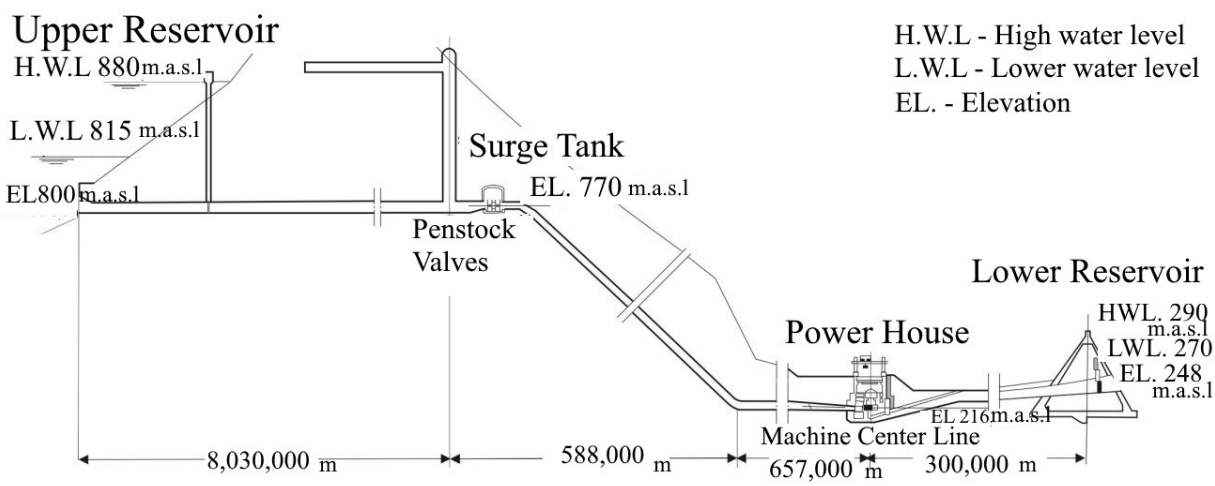

Fig. 1. *PSP Bajina Basta, Serbia – system disposition*

building; and a lower exit-entrance building located in the lower reservoir of the RHPP on the upstream slope of the existing concrete dam of HPP Bajina Basta, as shown in Fig. 1. According to the basic technical data of PSP, the plant has a total installed capacity of 630 MW (two units of 315 MW each), an average annual production of 1070 GWh, a useful accumulation volume of 150 × 10^6 m^3, a maximum net head of 600 m, and an installed discharge of 126 m^3/s.

2 4Q CHARACTERISTICS REPRESENTED BY *Wh* AND *Wm* SUTER CURVES FOR 3 PUMP-TURBINE MODELS

The performance curves corresponding to the 3 specific speeds nq = 27, nq = 38, and nq = 50 used in this paper were also incorporated into the performance curve analyses published in [6].

The specific speed is defined as:

$$nq = n\frac{\sqrt{Q}}{H^{3/4}}, \tag{1}$$

where nq is the specific speed [-], n is the speed of rotation (rpm,, Q is the discharge [m^3/s] and H is the rated head [m]. The Eq. (1) is used for calculation the nq specific speed [-] of the pump turbines (for turbine mod – rated head).

The Suter curves shown in Figs. 3 to 8 were obtained by converting the 4Q characteristics Q_{11}, n_{11}, and M_{11} (for different openings of the wicket gates), and 4Q characteristics $Q_{11} = Q/D_1 \times \sqrt{H}$, $n_{11} = n^x D_1/\sqrt{H}$, and $M_{11} = M/D_1{}^{3x}\sqrt{H}$ based on laboratory test data. Then, the points of highest efficiency for all four quadrant curves for various openings of guide vanes of pump-turbine models are determined and the one for the pump mode is chosen as the reference one. So, the data for H^*, Q^* and M^* from the optimum point of the pump-turbine model are further used in process of data conversion. Next, the values for H, M and Q for each point on the 4Q curve are calculated for each of the openings of the guide vanes of the model machine. After this procedure, the calculation of values for h, β, α and v is conducted, where the relative head, is $h = H/H^*$, the relative moment $\beta = M/M^*$, the relative speed $\alpha = n/n^*$, and the relative discharge $v = Q/Q^*$. The complete conversion procedure is presented in [6], where the $Wh(\theta) = h/(\alpha^2 + v^2)$ are curves of the head characteristics and $Wm(\theta) = \beta/(\alpha^2 + v^2)$ curves of the torque characteristics, are expressed in the function of the angle θ defined as $\theta = arctg\ \alpha/v$. Suter curves are also presented for sixteen pump-turbine models and twenty-one pump models. Fig. 2 shows a sketch of the steps in the previous procedure of conversion from the 4Q curves with coordinates Q_{11}, n_{11}, M_{11} of the model into the Suter curves. Descriptions of the model laboratory tests and the method for obtaining the 4Q characteristics Q_{11}, n_{11}, and M_{11} may be seen in [42]. Additionally, the *Wh* and *Wm* Suter curves for nine models of radial pump-turbines are presented in [43].

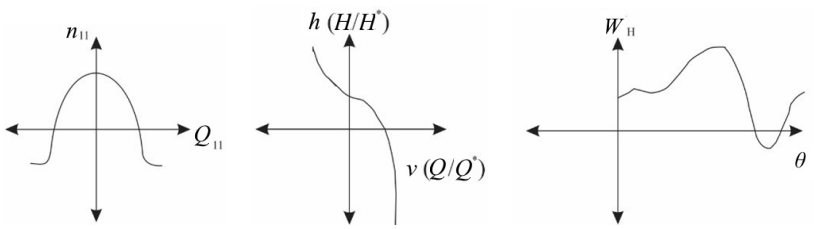

Fig. 2. *Graphic representation of the transition path from the values ($n_{11} - Q_{11}$)-model to the values ($H/H^* - Q/Q^*$)-model and then on the values ($Wh - \theta$)-model, (sketch of the calculation procedure)*

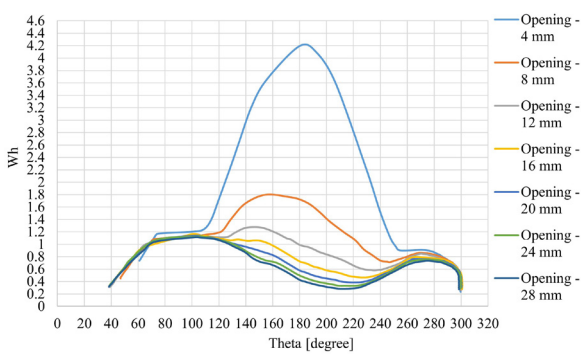

Fig. 3. *Wh* Suter curve for pump-turbine nq = 27 at PSP

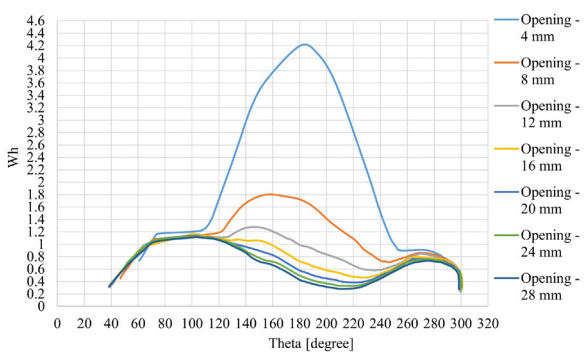

Fig. 4. *Wm* Suter curve for pump-turbine nq = 27 at PSP

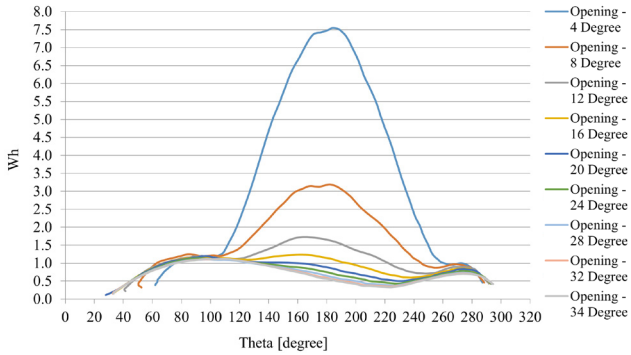

Fig. 5. *Wh* Suter curve for pump-turbine *nq* = 38 at PSP

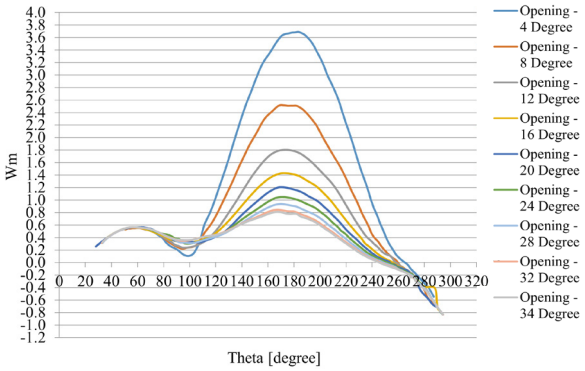

Fig. 6. *Wm* Suter curve for pump-turbine *nq* = 38 at PSP

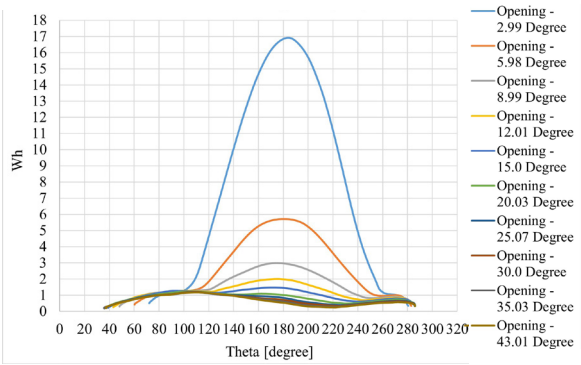

Fig. 7. *Wh* Suter curve for pump-turbine *nq* = 50 at PSP

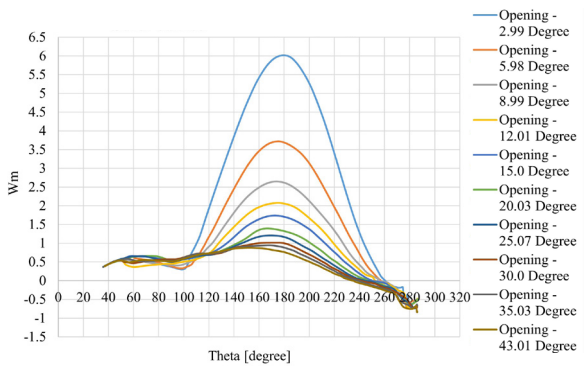

Fig. 8. *Wm* Suter curve for pump-turbine *nq* = 50 at PSP

The complete operating characteristics of pumps and pump-turbines with various specific speeds are not readily available. In general, the manufacturer supplies the head, brake horsepower, and the efficiency plotted against the discharge for the normal speed of operation. From these data, the characteristics of normal pump operation may be determined. However, it is necessary to have the complete characteristics of a pump and pump-turbines to determine the operation for all possible steady state conditions, or to determine transient conditions for normal or abnormal operations. The complete characteristics of a pump and pump-turbines consist of the zones of pump operation, turbine operation, and energy dissipation. These zones can be plotted as families of speed-ratio curves and torque-ratio curves on a (flow ratio-head ratio) coordinate system. In this form it is convenient to determine the transient water-hammer effects by graphical procedures. In addition, it is possible to determine by inspection the steady-state conditions existing at different heads or speeds under normal and abnormal conditions of operation.

3 GOVERNING EQUATIONS FOR MODELING TRANSIENT FLOWS AND THEIR NUMERICAL CALCULATION

In the one-dimensional (1D) mathematical model, the hydraulic system of PSP Bajina Basta is presented as a set of nodes (pump-turbines, surge tanks, storage basins, valves, and gates) connected by lines (tunnels, penstocks, pipes, and draft tubes).

A transient process occurs when the wicket gates are closing, and the resulting unsteady flow is described by the following equations in [7]:

- the equation of motion:

$$g\frac{\partial h}{\partial x}+v\frac{\partial v}{\partial x}+\frac{\partial v}{\partial t}+\frac{f}{2d}v|v|=0, \tag{2}$$

- the continuity equation:

$$\frac{\partial h}{t}+v\frac{\partial h}{\partial x}+\frac{a^2}{g}\frac{\partial v}{\partial x}-v\cdot\sin\alpha=0, \tag{3}$$

where v is the flow velocity [m/s], h is the piezometric head [m], a is the propagation velocity of circulation resulting wave [m/s], g is the acceleration due to gravity [m²/s], f is the Darcy-Weisbach friction factor, x is the spatial coordinate, d is the diameter of the

penstock [m], t is the time [s] and α is the inclination of the penstock in relation to the horizontal plane.

Eqs. (2) and (3) are partial differential equations of hyperbolic type. In the "x, t" plane there are two sets of lines, called "characteristic lines", defined by Eq. (4):

$$\frac{dx}{dt} = v \pm a. \tag{4}$$

Along these lines Eqs. (2) and (3) become ordinary differential equations, better suited for numerical integration. Details may be found in **[7]**.

Along a characteristic $dx/dt = v+a$:

$$\frac{g}{a}\frac{dh}{dt} + \frac{dv}{dt} - \frac{g}{a}v \cdot \sin\alpha + \frac{f}{2d}v|v| = 0. \tag{5}$$

Along a characteristic $dx/dt = v–a$:

$$-\frac{g}{a}\frac{dh}{dt} + \frac{dv}{dt} - \frac{g}{a}v \cdot \sin\alpha + \frac{f}{2d}v|v| = 0. \tag{6}$$

The boundary conditions at each node (pump-turbine) are analyzed. This mathematical model is based on the pump-turbine model test (the 4Q characteristics are presented in the form of *Wh* and *Wm* Suter curves) and the dynamic equation related to the unit, Eq. (7). Each component of the hydraulic system of PSP is included with the corresponding equations.

The authors developed a numerical code for calculating transient processes based on the MOC **[7]**, which was then upgraded with the following analysis of governor behavior.

Eq. (7) models the temporary speed droop governor with all its nonlinearities, where T_a is the time constant of the machine [s], ω^* is the normalized rotor angular speed [-], m_t is the unit hydraulic torque [-], m_e is the unit electrical torque [-], and D is the damping coefficient [-]:

$$T_a \frac{d\omega^*}{dt} = m_t - m_e - D\left(\omega^* - 1\right). \tag{7}$$

Eq. (8) represents the auxiliary servomotor and integrator, where y_1 is the auxiliary servomotor stroke [-], T_{y1} is the servomotor time constant [s], b_p is the permanent speed droop [-], K is the integrator gain [-], c is the command signal [-], e is the output of the temporary speed droop [-]:

$$\frac{dy_1}{dt} = -\frac{1}{T_{y1}}\left(1 + b_p K\right)y_1 - \frac{K}{T_{y1}}\left(\omega^* - c\right) - \frac{K}{T_{y1}}e,$$
$$0 < y_1 < 1. \tag{8}$$

Eq. (9) represents the temporary droop feedback, where T_d is the temporary speed droop time constant [s], b_t is the temporary speed droop [-]:

$$\frac{de}{dt} = -\left(\frac{1}{T_d} + \frac{b_t K}{T y_1}\right)e - \frac{b_t}{T_{y_1}}\left(1 + b_p K\right)y_1 - \frac{b_t K}{T_{y_1}}\left(\omega^* - c\right). \tag{9}$$

Eq. (10) represents the guide vane servomotor, where a_o is guide vane opening [mm] is given as a function of y servomotor stroke [-], Ty is the servomotor time constant [s]. The details may be found in **[7]** and **[44]**.

$$\frac{dy}{dt} = \frac{1}{T_y}\left(y_1 - y\right), 0 \le y \le 1, \left|\frac{dy}{dt}\right| \le \left(\frac{dy}{dt}\right)_{\max}. \tag{10}$$

4 DISCUSSIONS ON INFLUENCE OF SPECIFIC SPEED ON TRANSIENT PROCESSES

4.1 Basic Parameters

The calculation results for the transient processes of the two pump-turbines installed at HPSP Bajina Basta are presented for simultaneous load rejection – namely, of pump-turbine 1 from a power of 281 MW (turbine mode) and of pump-turbine 2 from a power of 284 MW (turbine mode) (the powers measured when performing real load rejection). For nq = 27 (the original specific speed of the pump-turbines at the PSP), the calculated results can be compared with those obtained by on-site measurements, while for nq = 38 and nq = 50, only the calculation results can be presented. Table 1 shows the basic data for the analyzed pump-turbines, where D_r is the inlet diameter of the runner and has the values of 4.82 m, 4.86 m, and 5.259 m for these three different nq runners, Q_r is the rated discharge and has the values of 63.1 m³/s, 96.3 m³/s, and 176.1 m³/s, H_r is the rated head and has the values of 554.3 m, 447 m, and 195 m respectively, and all these values are used for calculating the nq specific speed [-], according to Eq. (1).

The moment of inertia of rotating masses of HPSP is 1625×10³ kg×m². The initial values of net head 552.56 m, discharge 61 m³/s and rotational speed 428.57 rpm of pump-turbine units 1 and 2 are used in the numerical analysis.

Table 1. *Data for the three-prototype pump- turbines for the turbine mode of operation*

nq [-]	27	38	50
Dr [m]	4.82	4.86	5.259
Qr [m³/s]	63.1	96.3	176.1
Hr [m]	554.3	447	195
n [rpm]	428.6	375	250
Pr [MW]	294	382.7	306

The reason using these different specific speeds is that *nq* has a significant influence on the transient processes of pump-turbines based on the calculation results, is because of the next, very large difference in the ratio of inlet/outlet pump-turbine diameter, channel shape, and the other parameters of constructions of these three models of pump-turbines which is discussed in this paper. All the factors mentioned above have a bearing on the shape of the four-quadrant characteristics of these three models of pump-turbines which can be clearly seen in Figs. 14 to 19, especially in the area where the working point moves from the turbine zone (III) to the reverse pump zone (IV). In the area where the working point moves from the turbine zone (III) to the reverse pump zone (IV), the pump turbines operate along the characteristic S-shaped curve..

4.2 Calculated Performance Characteristics and Their Physical Behavior

Fig. 9 presents the curves of the head changes in spiral casings of pump-turbines 1 and 2 obtained by calculating the transient processes for all three specific speeds; the on-site measurements for each specific speed are also shown for comparison. In addition to the characteristics of the curves in certain zones, the influence of the specific speed is reflected by the different peak values. For instance, for pump-turbine 1 in the interval from 7 s to 11 s, a maximum pressure of 825 m was measured for nq = 27, while maximum pressures of 940 m, 1175 m, and 1025 m were calculated for nq = 27, nq = 38, and nq = 50, respectively. For pump-turbine 2 in the interval from 7 s to 11 s, a maximum pressure of 840 m was measured for nq = 27, while maximum pressures of 943 m, 1085 m, and 1010 m were calculated for nq = 27, nq = 38 and nq = 50, respectively.

Fig. 10 shows the curves of the change in discharge at pump-turbines 1 and 2 calculated under the same load rejection conditions. For pump-turbine 1 in the interval from 7 s to 11 s, for nq = 27, the discharge changes direction with the occurrence of reverse discharge (the operating point moves from the turbine zone to the reverse pump zone) and reaches a maximum of –31 m³/s in the reverse pump zone, which leads to pump-turbine instability. For; nq = 38, the discharge also changes direction (from the turbine zone to the reverse pump zone) and reaches a maximum of –32 m³/s in the reverse pump zone, which also leads to pump-turbine instability. For; nq = 50, the discharge also changes direction and reaches a maximum of –20 m³/s in the reverse pump zone, again leading to instability.

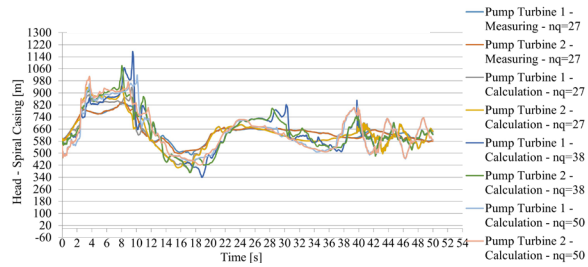

Fig. 9. Head in the spiral casing at PSP: transient process (simultaneous load rejection of pump-turbine 1 from a power of 281 MW and pump-turbine 2 from a power of 284 MW), measurements and calculations for nq = 27, only calculations for nq = 38 and nq = 50

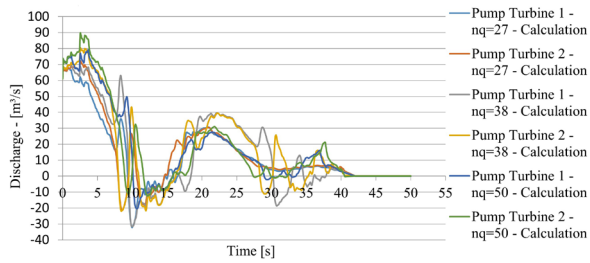

Fig. 10. Discharge at PSP: transient process (simultaneous load rejection of pump-turbine 1 from a power of 281 MW and pump-turbine 2 from a power of 284 MW); calculations for nq = 27, nq = 38, and nq = 50

For pump-turbine 2 in the interval from 7 s to 11 s, for nq = 27, the discharge changes direction (from the turbine zone to the reverse pump zone) and reaches a maximum of -23 m³/s in the reverse pump zone, which leads to the instability of pump turbine 2. For; nq = 38, the discharge similarly changes direction (from the turbine zone to the reverse pump zone) and reaches a maximum of –24 m³/s in the reverse pump zone, which also leads to instability of the pump-turbine. For; nq = 50, the discharge changes direction (from the turbine zone to the reverse pump zone) and reaches a maximum of –12 m³/s in the reverse pump zone, again leading to instability of the pump-turbine. In the interval from 7 s to 11 s, the pump-turbines 1

and 2 operated along the characteristic where the curve has an S-shape, which leads to difficulties during the load-rejected process, and are manifested by an unusual increase in water pressure, which leads to an increase in machine vibrations, and threatens the stability of the machine.

Fig. 11 presents the curves of the wicket gate openings for pump-turbines 1 and 2 obtained by calculating the transient processes; the on-site measurements are shown for comparison. For nq = 27, the curves of the wicket gate openings for both pump-turbines are obtained both by transient process calculations and by on-site measurements, while for nq = 38 and nq = 50, the wicket gate opening curves for both pump-turbines are obtained only by calculating the transient process. The curves of the wicket gate openings for both pump-turbines calculated for nq = 27, nq = 38, and nq = 50 are slightly different from the on-site measurement curves of the wicket gate openings for nq = 27. The presented trends of the wicket gate closing for pump-turbines 1 and 2 for nq = 27, nq = 38, and nq = 50 comprise three steps: the first step is a wicket gate opening of 90 % to 60 %, the second step is an opening of 60 % to 10 %, and the third step is an opening ranging from 10 % to 0 %. The total closing time for the completion of all three steps is 42 s.

Fig. 12 plots the curves reflecting the changes in the speed of rotation of pump-turbines 1 and 2 obtained both by calculations and by on-site measurements. For pump-turbine 1 in the interval from 7 s to 11 s, for nq = 27, the maximum measured speed of rotation was 575 rpm, while the maximum calculated speeds of rotation were 608 rpm, 697 rpm, and 702 rpm for nq = 27 for nq = 38, and nq = 50, respectively. For pump-turbine 2 in the interval from 7 s to 11 s, for nq = 27, the maximum measured speed of rotation was 577 rpm, while the maximum calculated speeds of rotation were 619 rpm, 678 rpm, and 699 rpm for nq = 27, nq = 38, and nq = 50, respectively.

Fig. 13 presents the curves of the calculated changes in the head within the draft tubes of pump-turbines 1 and 2. For pump-turbine 1 in the interval from 7 s to 11 s, the minimum calculated pressures were 20 m, -40 m, and -34 m for nq = 27, nq = 38, and nq = 50, respectively. For pump-turbine 2 in the interval from 7 s to 11 s, the minimum calculated pressures were 0.5 m, –50 m, and –15 m for nq = 27, nq = 38, and nq = 50, respectively. The physical results obtained during transient processes clearly

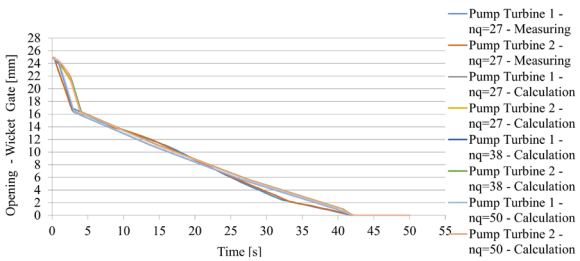

Fig. 11. *Wicket gate opening at PSP: transient process (simultaneous load rejection of pump-turbine 1 from a power of 281 MW and pump-turbine 2 from a power of 284 MW); measurements for* nq *= 27, calculations for* nq *=27,* nq *= 38, and* nq *= 50*

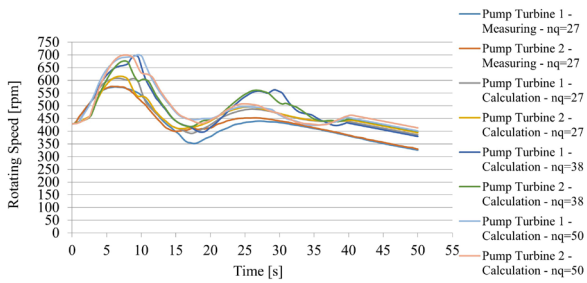

Fig. 12. *Speed of rotation at PSP: transient process (simultaneous load rejection of pump-turbine 1 from a power of 281 MW and pump-turbine 2 from a power of 284 MW); measurements for* nq *= 27, calculations for* nq *= 27,* nq *= 38, and* nq *= 50*

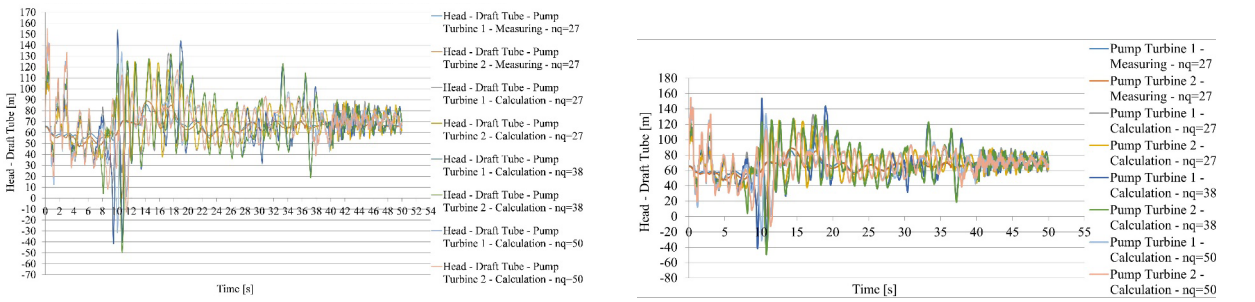

Fig. 13. *Head in the draft tube at PSP: transient process (simultaneous load rejection of pump-turbine 1 from a power of 281 MW and pump-turbine 2 from a power of 284 MW); measurements for* nq *= 27, calculations for* nq *= 27,* nq *= 38, and* nq *= 50*

show the influence of different specific speeds (*nq*) on the variations in the head within the spiral casing, head within the draft tube, speed of rotation, and discharge.

A detailed analysis of inlet conditions which was used during the simultaneous load rejection of pump-turbine 1 from a power of 281 MW and pump-turbine 2 from a power of 284 MW) was performed. Measurements for nq = 27, calculations for nq = 27, nq = 38, and nq = 50, confirmed that the same inlet conditions are used. In Figs. 9, 10, and 13 it is not easy to see the values of the initial conditions for the head in the spiral casing, discharge or the, head in the draft tube. This is because when starting the transient process the values for the head in the spiral casing, discharge,head in the draft tube for very short time 0.1 s the change the values and this is very difficult to see on diagrams presented on Figs. 9, 10, and 13

In Fig. 13 we can see that for pump-turbine 1 in the interval from 7 s to 11 s, the minimum calculated pressures were 20 m, –40 m, and –34 m for nq = 27, nq = 38, and nq = 50, respectively. For pump-turbine 2 in the interval from 7 s to 11 s, the minimum calculated pressures were 0.5 m, –50 m, and –15 m for nq = 27, nq = 38, and nq = 50, respectively. And the conclusion is the next: in the interval from 7 s to 11 s the pump-turbine 1 and 2 during the transient process coming in instability zone - coming in the instability zone of the S characteristic., the working point is moving from the turbine zone (III) to the reverse pump zone (IV). During this period the pump-turbines operated along the characteristic S-shaped curve). This is the reason why the head within the draft tubes of pump-turbines 1 and 2 for nq = 38 and nq = 50 arrives at the maximum negative values of –50 m. This clearly explains how much show the influence of different specific speeds (*nq*) on the variations in the head within the draft tube.

The level for pressure taps in the draft tube is 212 m above sea level, and the axis of the runner of the pump-turbine is 216 m above sea level. As discussed, it is clear that the pressure head in the draft tube is well below the liquid vapour pressure head which is physically not possible. The authors provide the following explanation related to this phenomenon: this effect does not influence the bulk pressure history significantly as our investigation has been focused on the effect of the machine characteristics.

4.3 Working Point Trajectories During Transient Processes and Discussion of Operating Regimes

The trajectories of the working points (operating regimes) of pump-turbines 1 and 2 for nq = 27 during the transient process (simultaneous load rejection of pump-turbine 1 from a power of 281 MW in turbine mode and pump-turbine 2 from a power of 284 MW in turbine mode) are shown in Figs. 14 and 15 as traced in their four quadrant characteristics diagram. The transient process starts in the turbine zone. Next, for both pump-turbines, the working point moves through the turbine zone and subsequently enters and moves within the reverse pump zone, which means that instabilities during operation will occur while working in this zone.

As is clearly present in Figs. 14 and 15 for pump-turbine 1, the working point reaches its most distant position (Q_{11}/Q_{11o} = 0.56, n_{11}/n_{11o} = –1.19) in 8.9 s, while that of pump-turbine 2 reaches its most distant position (Q_{11}/Q_{11o} = 0.38, n_{11}/n_{11o} = –1.11) in 10.3 s. Figs. 14 and 15 clearly show that pump-turbine 1 at 8.9 s and pump-turbine 2 at 10.3 s, operating along the characteristic where the curve has an S-shape, will have difficulties during the load-rejected process,

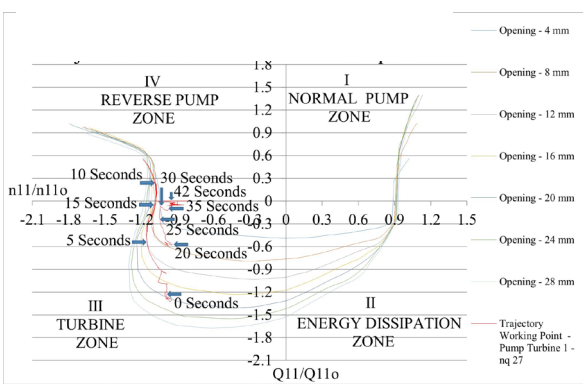

Fig. 14. *Trajectories of the working point of pump-turbine 1 at PSP during the transient process (simultaneous load rejection of pump-turbine 1 from a power of 281 MW and pump-turbine 2 from a power of 284 MW); calculation results for* nq *= 27*

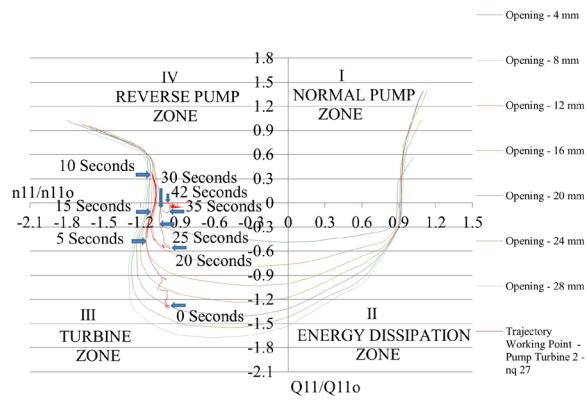

Fig. 15. *Trajectories of the working point of pump-turbine 2 at PSP during the transient process (simultaneous load rejection of pump-turbine 1 with a power of 281 MW and pump-turbine 2 with a power of 284 MW); calculation results for* nq *= 27*

which are manifested by an unusual increase in water pressure in the spiral case, which then leads to an increase in machine vibrations, and finally leads to a drop in the pressure in draft tube and threatens the stability of the machine.

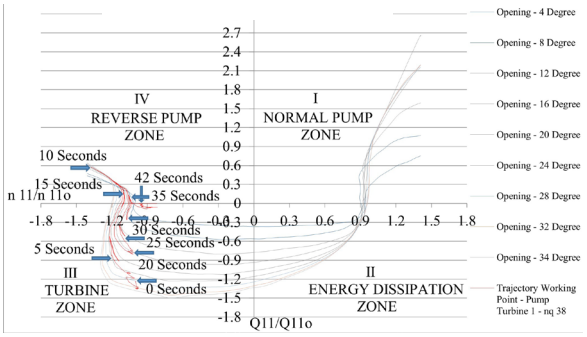

Fig. 16. *Trajectories of the working point of pump-turbine 1 at PSP during the transient process (simultaneous load rejection of pump-turbine 1 from a power of 281 MW and pump-turbine 2 from a power of 284 MW); calculation results for nq = 38*

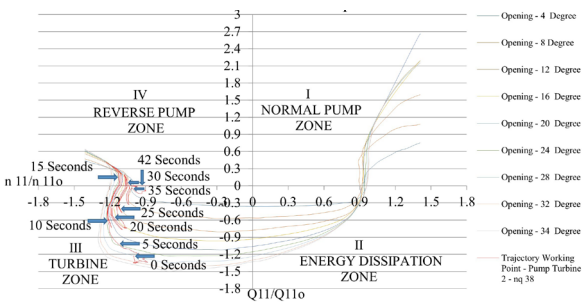

Fig. 17. *Trajectories of the working point of pump-turbine 2 at PSP during the transient process (simultaneous load rejection of pump-turbine 1 from a power of 281 MW and pump-turbine 2 from a power of 284 MW); calculation results for nq = 38*

Figs. 16 and 17 show the trajectories of the transient working points of pump-turbines 1 and 2, respectively, for $nq = 38$. The transient working points both start in the turbine zone. For pump-turbine 1, the working point moves through the turbine zone and then enters the reverse pump zone. In 10.1 s, the working point reaches its most distant position ($Q_{11}/Q_{11o} = 0.57$, $n_{11}/n_{11o} = -1.37$) in the reverse pump zone, which leads to the unstable operation of pump-turbine 1. Similarly, for pump-turbine 2, the working point moves through the turbine zone and then enters the reverse pump zone. In 11.5 s, the working point reaches its most distant position ($Q_{11}/Q_{11o} = 0.42$, $n_{11}/n_{11o} = -1.23$) in the same zone, leading to instability during the operation of pump-turbine 2. Figs. 16 and 17 clearly present that pump-turbine 1 at 10.1 s and pump-turbine 2 at 11.5 s, operating along the characteristic where the curve has an S-shape, have difficulties during the load-rejected process, which are manifested by an unusual increase in water pressure in the spiral case and, leads to an increase in machine vibrations. This then leads to a drop of pressure in the draft tube below the values of the vacuum and starts the process of cavitation on the runner, which threatens the stability of the machine. During the period of operating pump-turbine 2 (for $nq = 27$) along the characteristic where the curve has an S-shape, the maximum pressure of 840 m was measured. When, maximum pressures of 943 m were calculated, the discharge changes direction (from the turbine zone to the reverse pump zone) and reaches a maximum of –23 m^3/s in the reverse pump zone, which leads to the instability of pump-turbine 2, when maximum calculated speeds of rotation were 619 rpm (max. measured values 577 rpm).

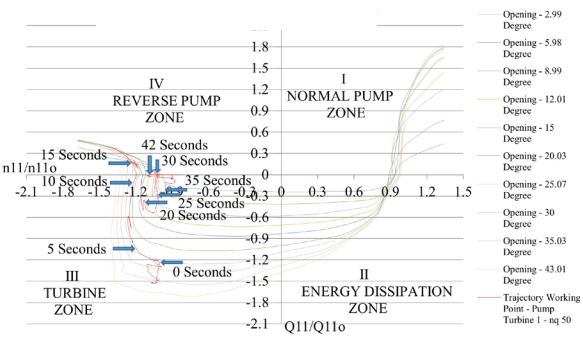

Fig. 18. *Trajectories of the working point of pump-turbine 1 at PSP during the transient process (simultaneous load rejection of pump-turbine 1 from a power of 281 MW and pump-turbine 2 from a power of 284 MW); calculation results for nq = 50*

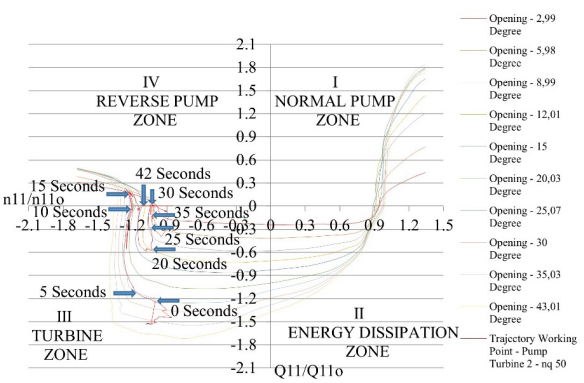

Fig. 19. *Trajectories of the working point of pump-turbine 2 at PSP during the transient process (simultaneous load rejection of pump-turbine 1 from a power of 281 MW and pump-turbine 2 from a power of 284 MW); calculation results for nq = 50*

Figs. 18 and 19 present the analog trajectories for $nq = 50$, for which the working points also start

in the turbine zone. The same movement trends may be noted for both working points, but they exhibit different peak points in the reverse pump zone: for pump-turbine 1, the peak is reached in 10.72 s at its most distant position (Q_{11}/Q_{11o} = 0.37, n_{11}/n_{11o} = –1.38), while for pump-turbine 2, the peak is reached in 11.8 s (Q_{11}/Q_{11o} = 0.23, n_{11}/n_{11o} = –1.26), which leads to the unstable operation of either turbine. Figs. 18 and 19 clearly present that pump-turbine 1 at 10.72 s and pump-turbine 2 at 11.8 s, operating along the characteristic where the curve has an S-shape, have difficulties during the load-rejected process, which are manifested by an unusual increase in water pressure in the spiral case, leading to an increase in machine vibrations, which then leads to a drop of pressure in the draft tube below the values of the vacuum starts the process of cavitation on the runner, and threatens the stability of the machine.

During the analyzed transient process span of 42 s, both working points move through the turbine zone, enter and remain for some period in the reverse pump zone, and then re-enter the turbine zone. Finally, when the discharge equals zero, the working points move along the n_{11}/n_{11o} axis until the pump-turbine stops, which occurs when the working point arrives at the zero point of the n_{11}/n_{11o} in Q_{11}/Q_{11o} coordinate system. The significant influences of the specific speed *nq* on the transient process can be seen from the presented diagrams and working points of all three models of pump-turbines coming in S-shaped zone.

5 REMARKS ON EXPERIMENTAL AND CALCULATION UNCERTAINTIES

Figs. 9 to 13 present comparisons between the measured and computed results for PSP in the case of the simultaneous load rejection of both pump-turbines. Generally, the computed results are confirmed by field tests. However, the comparison between the measured and computed results is hampered by uncertainties associated with these field tests. A common problem in water systems is that how much of air is trapped at certain locations in the system is unknown. During the transient process, in zones of low pressure, these dissolved gases can evolve. When small amounts of gas are released, the wave speed is greatly affected, and this phenomenon has considerable influences on the time and magnitude of pressure. In many cases, the actual characteristics of the pump-turbine, pump and turbine are not known in all working zones of the turbomachinery during failure. Since a computer simulation was performed in the absence of all the above parameters, it is difficult to expect that the calculated data will accurately match the field data, as there must be some error **[7].** During field measurements of the turbomachine main parameters (the heads in the spiral casing and draft tube, discharge, and speed of rotation), the expected error is between 1 % and 2 %. As shown in **[45],** the measurement errors during field measurements are ±1.2 % for the turbine efficiency, 0.866 % for the turbine power, 0.10 % for the turbine head or specific energy, and ±0.822 % for the turbine discharge).

6 CONCLUSIONS

The 4Q Suter curves for three pump-turbine models with specific speeds of *nq* = 27, *nq* = 38 and *nq* = 50 are presented and analyzed in this paper. These curves are used as input data for the numerical code to calculate the transient processes. The results of the calculations for PSP (spiral casing head, discharge, speed of rotation, and draft tube head) are mutually compared, revealing a significant difference among the results for the various specific speeds. The conclusion is that different specific speeds have significant influence on the transient processes of pump-turbines based on the calculation results.

Also, the important contribution of this paper is the detailed analysis of the trajectory of the working point for all three pump-turbine models during the transient process. The working point moves from the turbine zone (III) to the reverse pump zone (IV), while during this period the pump-turbines operated along the characteristic S-shaped curve. This led to difficulties during the load-rejection process manifested by an unusual increase in water pressure, and an increase in machine vibrations, threatening the machine stability. The analysis quantitatively revealed the negative impact of specific speed *nq* on this kind of machine behavior. The results carried out in this paper will be useful for the designers of pump-storage plants, allowing them to improve the selection of runners of the appropriate specific speed *nq*.

7 ACKNOWLEDGEMENTS

The special research, carried out on two pump-turbine models (*nq* = 38 and *nq* = 50) at the State Key Laboratory of Water Resources and Hydropower Engineering Science, Wuhan University, China, which provided the Q_{11}, n_{11}, and M_{11} 4Q characteristic data, is gratefully acknowledged.

8 NOMENCLATURES

a pressure wave velocity, [m/s]
a_0 guide vane opening, [mm], [-]
b_p permanent speed droop, [-]
b_t temporary speed droop, [-]
c command signal, [-]
d pipe diameter, [m]
D_r inlet diameter of runner, [m]
D damping coefficient, [-]
e output of the temporary speed droop, [-]
f coefficient of friction, [-]
g gravitational constant of acceleration, [m/s^2]
H_r rated head, [m]
h piezometric head, [m]
K integrator gain, [-]
M_{11} unit moment, [-]
m_t unit hydraulic torque, [-]
m_e unit electrical torque, [-]
nq specific speed, [-]
n speed of rotation, [rpm]
n_{11} unit speed of rotation, [-]
n_{110} rated unit speed of rotation, [-]
P_r rated power, [MW]
Q_r rated discharge, [m^3/s]
Q discharge, [m^3/s]
Q_{11} unit discharge, [-]
Q_{110} rated unit discharge, [-]
t time, [s]
T_a time constant of the machine, [s]
T_{y1}, T_y servomotor time constants, [s]
T_d temporary speed droop time constants, [s]
v velocity, [m/s]
W_h characteristic head, [-]
W_m characteristic moment, [-]
x coordinate measured along the pipe axis, [m]
y guide vane servomotor stroke, [-]
y_1 auxiliary servomotor stroke, [-]
ω^* normalized rotor angular speed, [-]
α inclination of the penstock in relation to the horizontal plane, [-]

9 REFERENCES

[1] Donsky, B. (1961). Complete pump characteristics and the effects of specific speeds on hydraulic transients. *Journal of Basic Engineering*, vol. 83, no. 4, p. 685-696, **DOI:10.1115/1.3662299**.

[2] Brown, R.J., Rogers, D.C. (1980). Development of pump characteristics from field tests. *Journal of Mechanical Design*, vol. 102, no. 4, p. 807-817, **DOI:10.1115/1.3254826**.

[3] Knapp, R.T. (1937). Complete characteristics of centrifugal pumps and their use in the prediction of transient behavior. *Transactions of ASME*, vol. 59, no. 8, p. 683-689, **DOI:10.1115/1.4020576**.

[4] Giljen, Z., Nedeljkovic, M. (2018). Radial hydraulic machinery four-quadrant performance curves dependent on specific speed and applied in transient calculations. *IOP 9IOP Conference Series: Earth and Environmental Science*, vol. 240, no, 4, art ID 042002, **DOI:10.1088/1755-1315/240/4/042002**.

[5] Thorley, A.R.D. (2004). *Fluid Transients in Pipeline Systems*. 2nd ed. Professional Engineering Publishing, London.

[6] Giljen, Z., Nedeljkovic, M., Cheng, Y.G. (2018). Analysis of four-quadrant performance curves for hydraulic machinery transient regimes. *17th International Conference on Fluid Flow Technologies Conference Proceedings*, paper no. 98.

[7] Wylie, E.B., Streeter, V.L. (1993). *Fluid Transients in Systems*. Prentice Hall, Upper Saddle River.

[8] Li, Z., Bi, H., Karney, B., Wang, Z., Yao, Z. (2017). Three-dimensional transient simulation of a prototype pump-turbine during normal turbine shutdown. *Journal of Hydraulic Research*, vol. 55, no. 4, p. 520-537, **DOI:10.1080/00221686.2016.1276105**.

[9] Giljen, Z. (2014). Numerical and field tests of hydraulic transients at Piva power plant. *IOP Conference Series: Earth and Environmental Science*, vol. 22, **DOI:10.1088/1755-1315/22/4/042010**.

[10] Giljen, Z. (2017). Pressure oscillations in Piva hydro power plant draft tube: case studies. *Proceedings of the ASME 2017 Fluids Engineering Division Summer Meeting*, art. ID V01AT03A014, **DOI:10.1115/FEDSM2017-69218**.

[11] Capponi, C., Zecchin, C.A., Ferrante, M., Gong, J.J. (2017). Numerical study on accuracy of frequency-domain modelling of transients. *Journal of Hydraulic Research*, vol. 55, no. 6, p. 813-828, **DOI:10.1080/00221686.2017.1335654**.

[12] Casartelli, E., Del Rio, A., Mangani, L., Schmid, A. (2022). Capturing the S-shape of pump-turbines by computational fluid dynamics simulations using an anisotropic turbulence model. *Journal of Fluids Engineering*, vol. 144, no. 2, art. ID 021203, **DOI:10.1115/1.4051809**.

[13] Deniz, S., Del Rio, A., Von Burg, M., Tiefenthaler, M. (2022). Investigation of the flow instabilities of a low specific speed pump-turbine part 1: Experimental and numerical analysis. *Journal of Fluids Engineering*, vol. 144, no. 7, art. ID 071209, **DOI:10.1115/1.4053900**.

[14] Fu, X., Zuo, Z., Chang, H., Li, D., Wang, H., Wei, X. (2021). Mechanism of low frequency high amplitude pressure fluctuation in a pump-turbine during the load rejection process. *Journal of Hydraulic Research*, vol. 59, no. 2, p. 280-297, **DOI:10.1080/00221686.2020.1780488**.

[15] Xia, L.S., Zhang, C.Z, Li, H. (2021). Influences of runner blade shape on the transient behaviours of pump-turbines in load rejection. *Journal of Hydraulic Research*, vol. 59, no. 3, p. 462-476, **DOI:10.1080/00221686.2020.1780503**.

[16] Zheng, X., Zhang, Y., Li, J., Zhang, Y. (2020). Influences of rotational speed variations on the flow-induced vibrational performance of a prototype reversible pump-turbine in spin-no-load mode. *Journal of Fluids Engineering*, vol. 142, no. 1, art. ID 011106, **DOI:10.1115/1.4045159**.

[17] Xia, L.S., Cheng, Y.G., Yang, J.D., Cai, F. (2019). Evolution of flow structures and pressure fluctuations in the S-shaped region of a pump-turbine. *Journal of Hydraulic Research*, vol. 57, no. 1, p. 107-121, **DOI:10.1080/00221686.2018.1459893**.

[18] Hu, J., Yang, J., Zeng, W., Yang, J. (2019). Constant-speed oscillation of a pump-turbine observed on a pumped-storage model system. *Journal of Fluids Engineering*, vol. 141, no. 5, art. ID 051109, **DOI:10.1115/1.4042763**.

[19] Li, D., Qin, Y., Zuo, Z., Wang, H., Liu, S., Wei, X. (2019). Numerical simulation on pump transient characteristic in a model pump-turbine. *Journal of Fluids Engineering*, vol. 141, no. 11, art. ID 111101, **DOI:10.1115/1.4043496**.

[20] Zhang, X., Zeng, W., Cheng, Y.G., Yang, Z., Chen, Q., Yang, J. (2019). Mechanism of fast transition of pressure pulsations in the vaneless space of a model pump-turbine during runaway. *Journal of Fluids Engineering*, vol. 141, no. 12, art. ID 121104, **DOI:10.1115/1.4044068**.

[21] Zhu, B., Tan, L., Wang, X., Ma, Z. (2018). Investigation on flow characteristics of pump-turbine runners with large blade lean. *Journal of Fluids Engineering*, vol. 140, no. 3, art. ID 031101, **DOI:10.1115/1.4037787**.

[22] Fu, X., Li, D., Wang, H., Zhang, G., Li, Z., Wei, X., Qin, D. (2018). Energy analysis in a pump-turbine during the load rejection process. *Journal of Fluids Engineering*, vol. 140, no. 10, art. ID 101107, **DOI:10.1115/1.4040038**.

[23] Ran, H., Luo, X. (2018). Experimental study of instability characteristics in pump-turbines. *Journal of Hydraulic Research*, vol. 56, no. 6, p. 871-876, **DOI:10.1080/00221686.2017.1422193**.

[24] Xiuli, M., Giorgio, P., Yuan, Z. (2018). Francis-type reversible turbine field investigation during fast closure of wicket gates. *Journal of Fluids Engineering*, vol. 140, no. 6, art. ID 061103, **DOI:10.1115/1.4039089**.

[25] Yexiang, X., Wei, Z., Zhengwei, W., Jin, Z., Soo-Hwang, A., Chongji, Z., Yongyao, L. (2018). Numerical analysis of the effect of misaligned guide vanes on improving S-shaped characteristics for a pump-turbine. *Journal of Fluids Engineering*, vol. 140, no. 3, art. ID 031102, **DOI:10.1115/1.4038077**.

[26] Xia, L.S., Cheng, Y.G., You, J., Zhang, X., Yang, J., Qian, Z. (2017). Mechanism of the S-shaped characteristics and the runaway instability of pump-turbines. *Journal of Fluids Engineering*, vol. 139, no. 3, art. ID 031101, **DOI:10.1115/1.4035026**.

[27] Xia, L.S., Cheng, Y.G., Yang, Z., You, J., Yang, J., Qian, Z. (2017). Evolutions of pressure fluctuations and runner loads during runaway processes of a pump-turbine. *Journal of Fluids Engineering*, vol. 139, no. 9, art. ID 091101, **DOI:10.1115/1.4036248**.

[28] Li, Z., Wang, Z., Wei, X., Qin, D. (2016). Flow similarity in the rotor-stator interaction affected region in prototype and model Francis pump-turbines in generating mode. *Journal of Fluids Engineering*, vol. 138, no. 6, art. ID 061201, **DOI:10.1115/1.4032298**.

[29] Zhang, X., Cheng, Y.G., Xia, L.S., Yang, J., Qian, Z. (2016). Looping dynamic characteristics of a pump-turbine in the S-shaped region during runaway. *Journal of Fluids Engineering*, vol. 138, no. 9, art. ID 091102, **DOI:10.1115/1.4033297**.

[30] Zeng, W., Yang, J., Hu, J., Yang, J. (2016). Guide-vane closing schemes for pump-turbines based on transient characteristics in S-shaped region. *Journal of Fluids Engineering*, vol. 138, no. 5, art. ID 051302, **DOI:10.1115/1.4032069**.

[31] Cavazzini, G., Covi, A., Pavesi, G., Ardizzon, G. (2016). Analysis of the unstable behavior of a pump-turbine in turbine mode: Fluid-dynamical and spectral characterization of the S-shape characteristic. Journal of Fluids Engineering, vol. 138, no. 2, art. ID 021105, **DOI:10.1115/1.4031368**.

[32] Zeng, W., Yang, J., Guo, W. (2015). Runaway instability of pump-turbines in S-shaped regions considering water compressibility. *Journal of Fluids Engineering*, vol. 137, no. 5, art. ID 051401, **DOI:10.1115/1.4029313**.

[33] Yu, X., Zhang, J., Miao, D. (2015). Innovative closure law for pump-turbines and field test verification. *Journal of Hydraulic Engineering*, vol. 141, no. 3, **DOI:10.1061/(ASCE)HY.1943-7900.000097**.

[34] Sun, H., Xiao, R., Liu, W., Wang, F. (2013). Analysis of S-characteristics and pressure pulsations in a pump-turbine with misaligned guide vanes. *Journal of Fluids Engineering*, vol. 135, no. 5, art. ID 051101, **DOI:10.1115/1.4023647**.

[35] Huang, W., Yang, K., Guo, X., Ma, J., Wang, J., Li, J. (2018). Prediction method for the complete characteristic curves of a Francis pump-turbine. *Water*, vol. 10, no. 2, art. ID 205, **DOI:10.3390/w10020205**.

[36] Pejovic, S., Krsmanovic, Lj., Jemcov, R., Crnkovic, P. (1976). Unstable operation of high-head reversible pump-turbines. *8th IAHR Symposium on Hydraulic Machinery Equipment and Cavitation*, Leningrad.

[37] Zeng, W., Yang, J., Cheng, Y.G. (2015). Construction of pump-turbine characteristics at any specific speed by domain-partitioned transformation. *ASME Journal of Fluids Engineering*, vol. 137, no. 3, art. ID 031103, **DOI:10.1115/1.4028607**.

[38] Meniconi, S., Brunone, B., Frisinghelli, M. (2018). On the role of minor branches, energy dissipation, and small defects in the transient response of transmission mains. *Water*, vol. 10, no. 2, art. ID 187, **DOI:10.3390/w10020187**.

[39] Simpson, A.R., Marchi, A. (2013). Evaluating the approximation of the affinity laws and improving the efficiency estimate for variable speed pumps. *Journal of Hydraulic Engineering*, vol. 139, no. 12, p. 1314-1317, **DOI:10.1061/(ASCE)HY.1943-7900.0000776**.

[40] Zhou, R., Chen, H., Dong, L., Liu, H., Chen, Z., Zhang, Y., Cheng, Z. (2022). Effect of vibration and noise measuring points distribution on the sensitivity of pump cavitation diagnosis. *Strojniški vestnik – Journal of Mechanical Engineering*, vol. 68, no. 5, p. 325-338, **DOI:10.5545/sv-jme.2022.59**.

[41] Soori, M., Asmael, M. (2021). Virtual minimization of residual stress and deflection error in the five-axis milling of turbine blades. *Strojniški vestnik – Journal of Mechanical Engineering*, vol. 67, no. 5, p. 235-244, **DOI:10.5545/sv-jme.2021.7113**.

[42] Giljen, Z., Nedeljkovic, M., Heninger, L. (2018). Complex testing on the installation of the radial pump-turbine model determination of four-quadrant characteristics. *International Conference Energy and Ecology Industry*, art. ID 1.3.

[43] Giljen, Z., Nedeljkovic, M., Cheng, Y.G. (2016). Pump-turbine characteristics for analysis of unsteady flows. *28th IAHR Symposium on Hydraulic Machinery and Systems*, art. ID 195.
[44] Obradovic, D., Arnautovic, D., Pejovic, S. (1988). Mathematical modeling of transient regimes in multi-unit hydro power plants. *XIV. IAHR Symposium on Hydraulic Machinery and Systems*, p. 163-176.
[45] Turboinštitut (2009). *PIVA HPP turbine site testing units 1, Report,* Ljubljana.